Metabolism

Molecular Cancer Research

Optical Imaging of Glucose Uptake and Mitochondrial Membrane Potential to Characterize Her2 Breast Tumor Metabolic Phenotypes

Megan C. Madonna[1], Douglas B. Fox[2], Brian T. Crouch[1], Jihong Lee[1], Caigang Zhu[1], Amy F. Martinez[1], James V. Alvarez[2], and Nirmala Ramanujam[1,2]

Abstract

With the large number of women diagnosed and treated for breast cancer each year, the importance of studying recurrence has become evident due to most deaths from breast cancer resulting from tumor recurrence following therapy. To mitigate this, cellular and molecular pathways used by residual disease prior to recurrence must be studied. An altered metabolism has long been considered a hallmark of cancer, and several recent studies have gone further to report metabolic dysfunction and alterations as key to understanding the underlying behavior of dormant and recurrent cancer cells. Our group has used two probes, 2-[N-(7-nitrobenz-2-oxa-1, 3-diaxol-4-yl) amino]-2-deoxyglucose (2-NBDG) and tetramethyl rhodamine ethyl ester (TMRE), to image glucose uptake and mitochondrial membrane potential, respectively, to report changes in metabolism between primary tumors, regression, residual disease, and after regrowth in genetically engineered mouse (GEM)-derived mammospheres. Imaging revealed unique metabolic phenotypes across the stages of tumor development. Although primary mammospheres overexpressing Her2 maintained increased glucose uptake ("Warburg effect"), after Her2 downregulation, during regression and residual disease, mammospheres appeared to switch to oxidative phosphorylation. Interestingly, in mammospheres where Her2 overexpression was turned back on to model recurrence, glucose uptake was lowest, indicating a potential change in substrate preference following the reactivation of Her2, reeliciting growth. Our findings highlight the importance of imaging metabolic adaptions to gain insight into the fundamental behaviors of residual and recurrent disease.

Implications: This study demonstrates these functional fluorescent probes' ability to report metabolic adaptations during primary tumor growth, regression, residual disease, and regrowth in Her2 breast tumors.

Introduction

Over 3 million women in the United States who have had breast cancer are at risk for developing recurrence (1). This risk is higher for women showing overexpression of Her2 (2). Women with Her2-positive ($Her2^+$) disease typically receive chemotherapy together with the anti-Her2 targeted therapy, trastuzumab, often in the neoadjuvant setting (3). Neoadjuvant therapy is used to make large or advanced tumors more operable and can also provide information on a tumor's response to therapy. At surgical resection, the extent of residual disease can be assessed using various metrics (4, 5). The absence of residual invasive disease in both the breast and axillary lymph nodes constitutes pathologic complete response and is positively associated with long-term relapse-free survival following adjuvant therapy (3). Almost half of $Her2^+$ patients who undergo the standard regime of neoadjuvant chemo- and anti-Her2 (trastuzumab) therapy, however, have residual disease at the time of surgery (6, 7). This partial response following neoadjuvant therapy leads to increased risk of relapse (4, 8). Further, approximately 30% of patients with breast cancer lacking any clinical or pathologic signs of metastasis at the time of diagnosis have disseminated tumor cells present in their bone marrow, which go undetected (9). Thus, residual disease owing to partial response at the primary tumor site may be viewed a surrogate for micrometastasis elsewhere in the body that may have also evaded neoadjuvant therapy and has the potential to eventually emerge as recurrent disease (10). The presence of residual disease at the primary tumor location or lack thereof not only informs local response to treatment but also distant disseminated tumor cells' therapy response. Residual tumor cells can persist in a dormant state for years prior to reemerging as a recurrent tumor (6, 8, 11). Given the large number of women at risk for recurrence, it is imperative to understand the fundamental behavior of these dormant residual cells; that is, to develop and adapt methodologies to visualize the pathways that are required for survival and recurrence of these cells *in vivo*, in hopes of one day designing and testing therapies to target these pathways to mitigate recurrence.

[1]Department of Biomedical Engineering, Duke University, Durham, North Carolina. [2]Department of Pharmacology & Cancer Biology, School of Medicine, Duke University, Durham, North Carolina.

Note: Supplementary data for this article are available at Molecular Cancer Research Online (http://mcr.aacrjournals.org/).

Current address of A.F. Martinez: Office of Research, Vanderbilt University Medical Center, Nashville, Tennessee.

Corresponding Author: Megan C. Madonna, Duke University, 1427 FCIEMAS, 101 Science Dr., Campus Box 90281, Durham, NC 27713. Phone: 919-660-8473; Fax: 919-684-4488; E-mail: megan.madonna@duke.edu

Mol Cancer Res 2019;17:1545–55

doi: 10.1158/1541-7786.MCR-18-0618

Metabolism may hold clues to dormant cell survival and recurrence because metabolic reprogramming has been observed in tumor cells that survive stressors such as changes in the environment or oncogene expression (12–14). Our group has previously shown acute Her2 oncogene downregulation results in a rapid decrease in 2[18F]fluorodeoxyglucose (FDG) uptake in PET *in vivo* in mammary tumors as well as in tumors driven by the Akt1, c-MYC, Wnt1, or H-Ras oncogenes in genetically engineered mouse (GEM) models, irrespective of the baseline FDG uptake (15). In another study, researchers used FDG-PET imaging of patients with Hodgkin lymphoma with suspected residual disease to determine recurrence risk. Here, elevated FDG intensity due to hypermetabolism was used to improve the diagnostic accuracy of determining whether a residual mass had relapsed; however, for one patient, relapsed residual disease was missed because of its small size (16). Moving beyond measuring glycolysis alone, other groups have shown transcriptome analysis of isolated residual cancer cell populations following MYC/Erbb2 oncogene inactivation in three-dimensional (3D) culture. Here, they demonstrate increased fatty acid synthase (FASN), oxidative phosphorylation, and elevated reactive oxygen species (ROS) compared with both normal and MYC/Erbb2-overexpressing tumor cells, highlighting the importance of mitochondrial metabolism following oncogene downregulation (17). These shifts were also found in transcriptomic and histologic changes between patient-matched diagnostic core-needle biopsies and neoadjuvant-treated surgical samples. Direct treatment of the increased ROS and dysregulated lipid metabolism with C75, an inhibitor of FASN, and etomoxir, a mitochondrial fatty acid oxidation inhibitor, in the experimental model attenuated tumor recurrence (17). In addition, others have reported the importance of the mitochondria in the regulation of the cell during periods of energy deprivation resulting in cell dormancy (18). Finally, recent work has shown potential metabolic vulnerabilities of the mitochondria in Her2 breast cancer tumors during treatment with Her2-targeted therapies (19). Taken together, these studies point to the significance of both mitochondrial metabolism and glycolysis in the metabolism of dormant cells.

In the studies described above, PET imaging was used to report on glucose uptake *in vivo*, and transcriptomics was used to examine oxidative phosphorylation of isolated residual cells (15, 17). Although transcriptomics, proteomics, and metabolomics provide a comprehensive approach to characterizing metabolic phenotypes of residual disease, they are limited to *in vitro* or *ex vivo* studies and cannot be used for repeated imaging sessions with multiple time points. Although PET imaging complements the "omic" technologies through live metabolic imaging, it is most commonly used to image a single endpoint and glucose uptake, providing a limited understanding of *in vivo* metabolism. Further, PET imaging, with a spatial resolution of 1 to 2 mm, does not have the resolution to specifically image the selective, highly localized alterations of a small population of dormant cells (20).

To achieve higher resolution, optical imaging has emerged as a strategy to quantify multiple metabolic pathways (21). Relying on endogenous fluorescence alone allows for imaging of flavin adenine dinucleotide (FAD) and reduced NADH to provide insight in the reduction–oxidation state in the electron transport chain with increased NADH fluorescence suggesting increased glycolysis and increased FAD fluorescence reflecting greater reliance on oxidative phosphorylation; however, they do not directly report on glucose uptake nor mitochondrial activity (22). Previously, our group has developed a novel technique to image glucose uptake and mitochondrial membrane potential (mitochondrial metabolism) using the fluorescent probes, 2-(N-(7-nitrobenz-2-oxa-1,3-diazol-4-yl)amino)-2-deoxyglucose (2-NBDG) and tetramethyl rhodamine ethyl ester (TMRE), respectively (23). Our group (24–27) and others (28–30) have extensively validated 2-NBDG imaging in cells (25), window chambers (24, 26), and flank tumor models (27). TMRE has been extensively used to study oxidative phosphorylation *in vitro* (31). Recently, we performed foundational studies to translate this indicator to quantitatively image oxidative phosphorylation *in vivo* (23, 32). This platform could be valuable in informing the evolution of disease and can inform which stages of the cancer cascade could be most susceptible to metabolically targeted therapy.

To study tumor dormancy and recurrence, we have developed a GEM model, *MMTV-rtTA;TetO-NeuNT (MTB;TAN*; ref. 33). Doxycycline administration induces expression of Her2/neu, leading to mammary tumor formation. Withdrawal of doxycycline leads to Her2 downregulation and tumor regression, mimicking sustained use of targeted therapies as would be the case in clinical practice (34). Residual cells surviving Her2 downregulation eventually reinitiate proliferation to form a recurrent tumor after 4 to 6 months, a similar timeframe to human breast cancer when correcting for mouse lifespan. Using this model, we and others have previously identified several genes that promote the survival and recurrence of residual cells, including par-4 (35), Snail (36), Ssb-1 (34), and Notch1 (37), which are all associated with recurrence in human breast cancer.

In this study, we demonstrate a strategy to dynamically image metabolic adaptions occurring during a tumor's transition from a primary tumor to residual disease using our Her2 model of tumor dormancy and previously validated metabolic probes. As a first step, we sought to examine these metabolic reporters with the GEM model *in vitro*. We generated primary mammosphere cultures from independent tumors harvested from MTB;TAN mice. Mammospheres were imaged first in the presence of doxycycline (Her2 on) to mimic a proliferating, primary tumor, and then 2 and 4 days following doxycycline withdrawal (Her2 off), to emulate tumor regression. Surviving residual tumor cells (14 and 28 days after doxycycline withdrawal) were also imaged. Finally, we resupplied doxycycline to residual cells and imaged the changes in metabolism during the transition from residual disease to recurrence. These time points were confirmed to model different stages of tumor development by immunofluorescent staining of Ki67 and cleaved caspase 3 (CC3). With mammospheres on doxycycline overexpressing Her2 (primary and reactivated), Ki67 expression was high, confirming proliferation. On the other hand, short-term doxycycline withdrawal resulted in increased CC3 expression, confirming apoptosis due to Her2 downregulation. Consistent with these findings, we show that mammospheres cultured continuously with doxycycline demonstrated the highest glycolytic rates compared with all other treatment groups, whereas short-term doxycycline removal (regression) yielded a dramatic increase in mitochondrial membrane potential. Increased mitochondrial membrane potential and decreased glucose uptake were maintained during dormancy. Interestingly, after the readdition of doxycycline to residual cells, mammospheres showed decreased glucose uptake but increased mitochondrial activity compared with the baseline proliferative state, indicating two metabolically distinct phenotypes. Interestingly, these two groups

had similar ATP levels and growth rates. This study reports the functional flexibility of these probes to report on different and distinct stages of tumor evolution and identifies key metabolic changes that occur over the course of tumor progression, dormancy, and recurrence with the ultimate goal of informing the potential impact of metabolically targeted therapies on this cancer cascade. Using these probes, we aim to create a nondestructive assay that can ultimately be translated to *in vivo* imaging using a mammary window chamber to image either GEM-derived or patient-derived xenograft models.

Materials and Methods

GEM model–derived mammospheres

Genetically engineered breast tumors were harvested from MTB;TAN mice, minced, and digested at 37°C in Earle's Balanced Salt Solution without phenol red media (Gibco 14155-063) supplemented with 300 U/mL collagenase and 100 U/mL hyaluronidase (StemCell 7912), 2% FBS (MediaTech 35-010-CV), 100 μg/mL gentamycin (Sigma G1264), 1% PenStrep (Gibco 15140-122), and 2 μg/mL doxycycline (RPI D43020). Dissociated tumor cells were cultured on Poly(2-hydroxyethyl methacrylate)-coated (Sigma P3932) dishes using RPMI media (Sigma R8758) supplemented with B27 (Invitrogen 17504-044), murine EGF (murine E4127), basic fibroblast growth factor (bFGF; Invitrogen 13256-029), PenStrep (Gibco 15140-122), and L-Glutamine (Gibco 25030-081; refs. 15, 34, 35). A total of 2 μg/mL doxycycline (RPI D43020) was added to the media to maintain the expression of Her2, a well-known oncogenic driver often amplified in aggressive breast cancers (38). To passage mammospheres, cells were collected, spun down, and trypsinized for 5 minutes until most cells were present as single cells. Trypsin was quenched using whole media, and cells were split 1:3. Mammospheres were passaged every 3 days. For experiments, mammospheres were trypsinized as above and allowed to grow for 2 days prior to experimental manipulations. To downregulate Her2 expression, mammospheres were transferred to media without doxycycline. To focus on the metabolic effects of modulating Her2 protein expression specifically, cells were cultured without EGF and bFGF for at least a week prior to experiments unless otherwise stated.

Metabolic imaging

Figure 1 details the different time points for metabolic imaging of glucose uptake and mitochondrial membrane potential. Cells were cultured with doxycycline to maintain Her2 tumor expression. Cells were grown without doxycycline in the media for each of the different time points (2, 4, 14, and 28 days). A separate culture was grown without doxycycline for 21 days and then returned to doxycycline 7 days before imaging. A total of 10 representative mammospheres from each time point were imaged, and all time points were measured on at least 2 different days, each as an independent experiment.

The fluorescent indicators, 2-NBDG and TMRE, were chosen for our imaging due to their translatability to *in vivo* experiments our group have previously published (23, 26, 39, 40). 2-NBDG Duke University Small Molecule Facility) is a fluorescent glucose analog that enters the cell via glucose transporters as a function of glucose uptake and causes an increase in fluorescence intensity (25, 41). TMRE (Life Technologies/Thermo Fisher Scientific) is a cationic dye that accumulates in the mitochondrial inner membrane as a function of mitochondrial membrane potential and causes an increase in fluorescence intensity (39, 42). During incubation, 2-NBDG and TMRE were diluted to final concentrations of 200 μmol/L and of 50 nmol/L, respectively, in media. Concentrations were chosen based on standard manufacturer protocols as to not affect the metabolism of cells and minimize each probe's toxicity (25).

Before imaging, the mammospheres were removed from media and washed with PBS. Cells were incubated at 37°C, 5% CO_2 for 30 minutes with either 200 μmol/L 2-NBDG or 50 nmol/L TMRE dissolved in glucose-free cell media. To prevent metabolite competition and minimize optical and biological cross-talk between metabolic probes, mammospheres were only stained with one of the two probes and different mammospheres were imaged at each time point. Mammospheres were then washed with PBS, returned to their normal media, and imaged immediately.

All images were collected on a Zeiss 780 Upright confocal microscope at the Duke University Light Microscopy Core Facility using a 20×/1.0 Water Zeiss W Plan-Apochromat 421452-9800 WD 1.8-mm objective and 2.0 digital zoom providing subcellular resolution (~0.4 μm). For 2-NBDG imaging, mammospheres

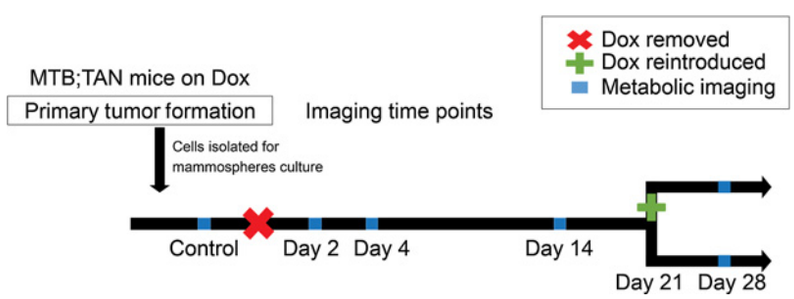

Figure 1.

Time course for metabolic imaging in 3D culture. Breast cancer cells were isolated and cultured with doxycycline (Dox) to maintain Her2 overexpression. To mimic therapeutic intervention, doxycycline was withdrawn for 2, 4, 14, or 28 days (indicated by red ×) to model tumor regression and dormancy. Imaging was performed before doxycycline withdrawal and at each time point using both 2-NBDG and TMRE as indicated by blue squares along the time course. After 21 days of doxycycline withdrawal, a separate culture had doxycycline added back to their growth media for 7 days (green + sign) to model recurrence.

were excited using a 488-nm argon laser source (Lasos) with emission collected from 494 to 560 nm. For TMRE imaging, mammospheres were excited using a 561-nm laser diode (Lasos) with emission collected from 565 to 691 nm. Fluorescence was detected using a GaAsP array and cooled photomultiplier tube. Image z stacks were taken starting from 1.5 μm above the mammosphere, through the entire sphere, and ending 1.5 μm below the mammosphere using a 1.5-μm step size for each image to adequately sample the entire sphere (Supplementary Fig. S1). The thickness of each image slice was 3.0 μm. The scan area at each plane was 212.5 × 212.5 μm (512 × 512 pixels) and took approximately 9 seconds to image per slice. A 512 × 512 × n data set, where n represents the number of slices needed to capture the entire mammosphere, was used for image processing. A fluorescence calibration standard slide (DeltaVision, Ex/Em: 488 nm/519 nm) was imaged at each session to account for day-to-day system variation using both imaging settings. Background fluorescence of media-only plates and unstained cell plates were obtained using each imaging setting to ensure background noise from the media, plate, or autofluorescence from endogenous fluorescence was negligible (<4%) over the linear range of the detector (data not shown).

Image processing

Overall uptake of 2-NBDG or TMRE was analyzed using MATLAB (MathWorks). A 3 × 3 × 3 median filter cube was applied to the entire cube to suppress the effects of shot noise. Because of the anisotropic resolution of confocal microscopy, the voxel size is anisotropic. To improve segmentation and image projections, a spline interpolation was performed in the z-direction to allow for a cubic voxel size of 0.42 μm^3 (17). From here, using MATLAB's Image Processing Toolbox, mammospheres were automatically segmented using the Fast Marching Method and intensities were corrected by a fluorescence calibration standard slide (43). A threshold of 1% of the maximum pixel value of the image was selected for the overall z-stack. All pixel values less than this threshold value were set to zero. Probability density functions (pdfs) were created from all nonzero pixels from each image sack for each group. All representative mammospheres shown throughout the manuscript are mean projections.

Immunofluorescence staining

Immunofluorescent staining of Ki67 and CC3 was performed to phenotype our mammospheres based on the proliferation (Ki67 staining) and apoptosis (CC3 staining) levels. Mammospheres were centrifuged (5 minutes, 1,500 × g) onto poly-D-lysine–coated coverslips (Neuvitro H-12-1.5-PDL). Cells were fixed with 4% paraformaldehyde (Thermo Fisher Scientific 28908) in PBS for 10 minutes, permeabilized with 0.05% Triton-X-100 (Sigma X-100) for 20 minutes, and then nonspecific binding was blocked with 10% normal goat serum (Invitrogen PCN5000) for 1 hour. To detect Ki67, cells were incubated with an anti-Kit67 antibody conjugated to Alexa Fluor 488 (1:100 dilution; BD Pharmingen #561165). To detect CC3, cells were incubated with rabbit anti-CC3 antibody (1:300; Cell Signaling Technologies 9661), followed by a goat anti-rabbit secondary antibody conjugated to Alexa Fluor 568 (1:200; Thermo Fisher Scientific #A-11011). Following incubation with antibodies, cells were mounted with ProLong Gold Antifade Reagent with DAPI (Cell Signaling Technology 8961).

CellTiter-Glo assay

To compare differences in 2-NBDG and TMRE uptake to changes in energy production, CellTiter-Glo Luminescent Cell Viability Assay (Promega) was used to quantify ATP levels following manufacturer instruction. Specifically, 2×10^5 cells per well were plated and grown for 2 days. Cells were harvested; half of all cells were used for ATP quantification, and half were used for protein content quantification. Luminescence was read on a luminometer and normalized to protein content for three biological replicates ($n = 3$). Data is shown as mean ± SEM.

qRT-PCR

qRT-PCR was completed to measure Her2 expression levels. Total RNA was initially extracted from cell pellets and reverse transcribed to cDNA. Threshold cycles of Erbb2 (Thermo Fisher Scientific, 4331182, Rn00566561_m1) were collected and normalized to β-actin (Thermo Fisher Scientific, 4331182, Mm02619580_g1) to calculate the ΔC_t values. $\Delta\Delta C_t$ values were calculated to determine the changes in Erbb2 levels between time points. The $2^{-\Delta\Delta C}{}_t$ was used to calculate fold changes in the target gene expression from three biological replicates, with each sample plated with three technical replicates ($n = 3$). To determine whether change in expression was biologically relevant, cells were plated at uniform density and counted after 1 and 4 days to identify proliferation rates. Data is shown as mean ± SEM from three independent experiments. ($n = 3$).

Statistical analysis

Pdfs were chosen to visualize the changes in fluorescence intensity distribution across different metabolic phenotypes. Empirical P values were calculated for a Kolmogorov–Smirnov statistic using blocked permutation ($n = 1{,}000$ random permutations per tests) to compare distributions, prior to binning data for graphing (44). To determine statistical significant changes in average probe uptake, Erbb2 expression, ATP production, and growth rates, mean values between time points were compared with Student t tests. Exact two-sided P values <0.05 were considered significant and are indicated as *. MATLAB (MathWorks) Statistics Toolbox was used for all tests.

Results

Media formulation and passage protocol validation produce reproducible metabolic endpoints.

Before studying metabolism during regression, dormancy, and recurrence, we validated media formulation and cell culture methodology to ensure reproducible and robust results. Mammospheres are normally maintained in culture media supplemented with bFGF and EGF (45, 46). Vander Heiden and colleagues have shown that growth factors can affect glycolysis (47), so we first evaluated the effect of these growth factors on 2-NBDG uptake between mammospheres cultured in doxycycline (primary mammospheres, control) and those removed from doxycycline for 2 days (regressing phenotype, test). Doxycycline withdrawal leads to rapid and total loss of Her2 protein (Supplementary Fig. S2). Given that growth factors promote tumor growth (48), we predicted that their presence would mask differences in tumor metabolism between the test and control group, specifically, glucose uptake between proliferative and regressing phenotypes. Imaging was performed on mammospheres continuously cultured with EFG and

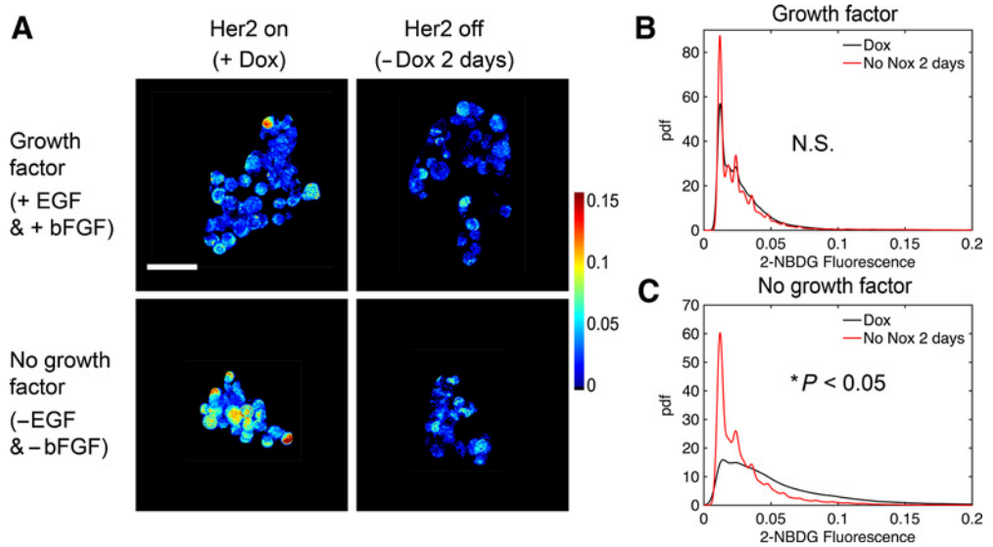

Figure 2.

Growth factors mask changes in glucose uptake following acute doxycycline withdrawal. 2-NBDG uptake was measured in cultures with doxycycline (control group) and cultures with doxycycline removed 2 days prior to imaging (test group). Fluorescence intensities were calibrated using a standard fluorescent slide and corrected for gain adjustments. **A,** Representative mean projection images of 2-NBDG intensity. **B,** pdfs of 2-NBDG pixel intensities from the 3D mammospheres show no significant difference between doxycycline and no doxycycline (Nox) for 2-day cultures with growth factors in the media. **C,** pdfs of 2-NBDG pixel intensities from the 3D mammospheres show significant differences between doxycycline and no doxycycline for 2-day cultures without the presence of growth factors in the media. For all groups, $n = 5$ mammospheres. (*, $P < 0.05$; N.S., not significant).

bFGF and on mammospheres cultured without EGF and bFGF for at least a week prior to imaging. Figure 2A shows representative images of mammospheres incubated with 200 μmol/L 2-NBDG as described previously. Qualitatively, only the mammospheres cultured without the added growth factors show a decrease in 2-NBDG intensity following doxycycline removal. To analytically assess 2-NBDG uptake, pdfs of 2-NBDG pixel intensities were created from images of mammospheres cultured with (Fig. 2B) and without growth factor in the media (Fig. 2C). There was no significant difference in 2-NBDG uptake between doxycycline and no doxycycline mammospheres grown in media with added growth factors. There was, however, a significant difference in 2-NBDG intensity between mammospheres on doxycycline and mammospheres following doxycycline removal when both were cultured without added growth factors ($P < 0.05$). The no growth factor condition was concordant with our previous *in vivo* study showing that Her2 downregulation caused decreased glucose uptake (15). Because the presence of growth factors masked metabolic changes caused by doxycycline withdrawal, all subsequent imaging studies were performed under conditions free of supplemental growth factors.

We next investigated whether continued passaging affects mammosphere metabolism. To explore how mammosphere phenotype is affected by the duration of time in culture, we varied the length of time mammospheres were serially passaged (every 3 days) on doxycycline prior to doxycycline withdrawal. Mammospheres were then incubated with either 200 μmol/L 2-NBDG or 50 nmol/L TMRE as described previously. Representative 2-NBDG and TMRE images in Fig. 3A show mammospheres serially passaged with doxycycline for variable lengths of time (passaged two, four, and six times) before doxycycline removal 2 days prior to imaging and show no qualitative differences in uptake. Pdfs of 2-NBDG and TMRE in Fig. 3B show no significant differences between passage times, indicating the length of passaging does not affect mammosphere metabolism. All subsequent imaging studies were performed with mammospheres cultured with doxycycline for 18 days or less.

2-NBDG and TMRE report on metabolic adaptations during transitions between primary tumors, regressing tumors, residual disease, and reinitiated tumor cells.

Having an optimized methodology to ensure biologically relevant, reproducible results, we next sought to assess how the metabolic properties of mammospheres change following doxycycline withdrawal (Her2 downregulation) and subsequent doxycycline readdition (Her2 reactivation). We performed immunofluorescence staining for Ki67 and CC3 to measure proliferation and apoptosis, respectively, as shown in Fig. 4A, to ensure the selected time points for our probes reported biologically relevant phenomena (primary tumor, regression, residual disease, and regrowth). Primary mammospheres ("P") grown in the presence of doxycycline (Her2 on) exhibited a proliferative phenotype with high Ki67 ($P < 0.05$) and low CC3 staining. (Supplementary Fig. S3 reports the quantification of Ki67 and CC3 results). Her2 downregulation led to decreased proliferation and increased apoptosis at 2 and 4 days following doxycycline withdrawal (early regression, "ER" and late regression, "LR"). Following these acute changes of regression, a population of residual mammosphere cells can survive Her2 downregulation (37). These residual mammospheres ("early residual disease" and "late residual disease"), assayed at 14 or 28 days following doxycycline withdrawal, exhibited low proliferation and low apoptosis, suggestive of a dormant state. Readdition of doxycycline led to the reinitiation of proliferation ($P < 0.05$) and regrowth of the mammospheres ("R").

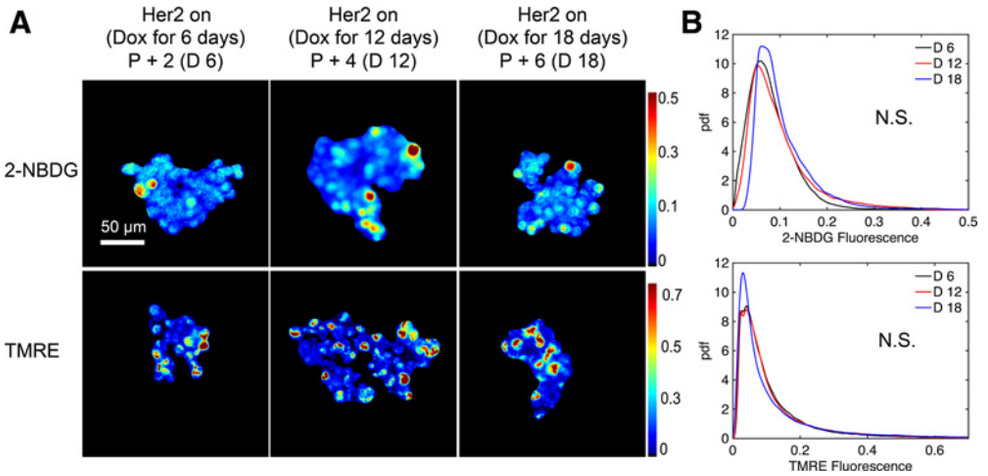

Figure 3.

Length of time in culture does not affect 2-day doxycycline withdrawal phenotype. Cells were cultured with doxycycline for 6, 12, or 18 days and passaged (P) every third day (P+2/D6, P+4/D12, or P+6/D18). Doxycycline was then removed from the media and metabolic imaging was performed 2 days later on days 8, 14, or 20, respectively. Fluorescence intensities were calibrated using a standard fluorescent slide and corrected for gain adjustments. **A,** Representative mean projection images of 2-NBDG and TMRE intensities 2 days following doxycycline withdrawal. **B,** pdfs of 2-NBDG and TMRE pixel intensities from the 3D mammospheres show no significant differences across varying lengths of time cells remained on doxycycline prior to removal. For all groups. $n = 5$ mammospheres. (*, $P < 0.05$; N.S., not significant).

We next performed metabolic imaging at each time point as described previously. Figure 4B shows representative two-dimensional (2D) projection images of 2-NBDG and TMRE intensities for mammospheres at baseline as well as 2, 4, 14 and 28 days following doxycycline removal and mammospheres cultured without doxycycline for 21 days and subsequently with doxycycline for 7 days (for comparison with the 28 day no doxycycline mammospheres). Qualitatively, primary mammospheres ("P", on doxycycline) show high 2-NBDG uptake and low TMRE uptake, characteristic of a primarily glycolytic phenotype; the proliferative nature of primary mammospheres is supported by Ki67 expression. On the other hand, mammospheres show a spike in mitochondrial membrane potential during late regression (4 days off doxycycline) characterized by high TMRE uptake. During the late regression stage, there also is increased CC3 expression. Taken together, this indicates a state of possible oxidative stress and metabolic alternations (49). Residual disease mammospheres ("early residual disease" and "late residual disease", 14 and 28 days off doxycycline) report moderate, stable signal levels of both probes with little Ki67 or CC3 expression. Following the readdition of doxycycline, Ki67 expression increases, indicating a stage of regrowth ("R", 21 days off doxycycline + 7 days on doxycycline), but decreased 2-NBDG and slightly elevated TMRE levels relative to the baseline proliferative state.

Pdfs of 2-NBDG and TMRE pixel intensities followed by a summary of all statistical comparisons for each probe across disease phases further indicate distinct changes throughout the tumor life cycle as shown in Fig. 4C. Pdfs were chosen to display and quantify the spatial heterogeneity that exists in each mammosphere; however, averages of each mammospheres' fluorescence are reported in Supplementary Fig. S4. In primary mammospheres ("P", on doxycycline), 2-NBDG intensity maximizes ($P < 0.05$) relative to all time points, whereas TMRE intensity is significantly decreased relative to mammospheres in all regressing ("early regression" and "late regression", 2 and 4 days off doxycycline) and residual disease ("early residual disease" and "late residual disease", 14 and 28 days off doxycycline) time points as determined by Kolmogorov–Smirnov testing. During regression ("early regression" and "late regression", 2 and 4 days off doxycycline), 2-NBDG intensity is significantly lower than primary mammospheres (on doxycycline; $P < 0.05$), whereas TMRE intensity increases and reaches a maximum ($P < 0.05$) in the late regression phase (4 days off doxycycline). These cells with increased TMRE uptake do not correspond to cells undergoing apoptosis (Supplementary Fig. S5). During the residual disease stages ("early residual disease" and "late residual disease", 14 and 28 days off doxycycline), 2-NBDG is increased relative to the regression phase, though not significantly, but remains decreased relative to that of the primary mammospheres ($P < 0.05$). On the other hand, TMRE is increased relative to baseline ($P < 0.05$) and the early regression phase ($P < 0.05$) and decreased relative to the late regression phase ($P < 0.05$). At 7 days after the readdition of doxycycline ("R"), mammospheres show both a significant decrease in 2-NBDG relative to all phases ($P < 0.05$) and TMRE uptake relative to regression and residual disease phases ($P < 0.05$), though higher TMRE uptake relative to primary mammospheres ($P < 0.05$).

In addition, primary and regrowing mammospheres had similar Erbb2 (i.e. Her2) gene expression, similar ATP content, and similar growth rates (Fig. 5A–C). Taken together, these findings suggest that tumor cell regrowth is associated with altered tumor cell metabolism but not with differences in the ability to proliferate in response to Her2 expression following long-term doxycycline withdrawal.

Discussion

Despite the increased interest in the regulation and function of metabolism in cancer, there still exists a need for a translational

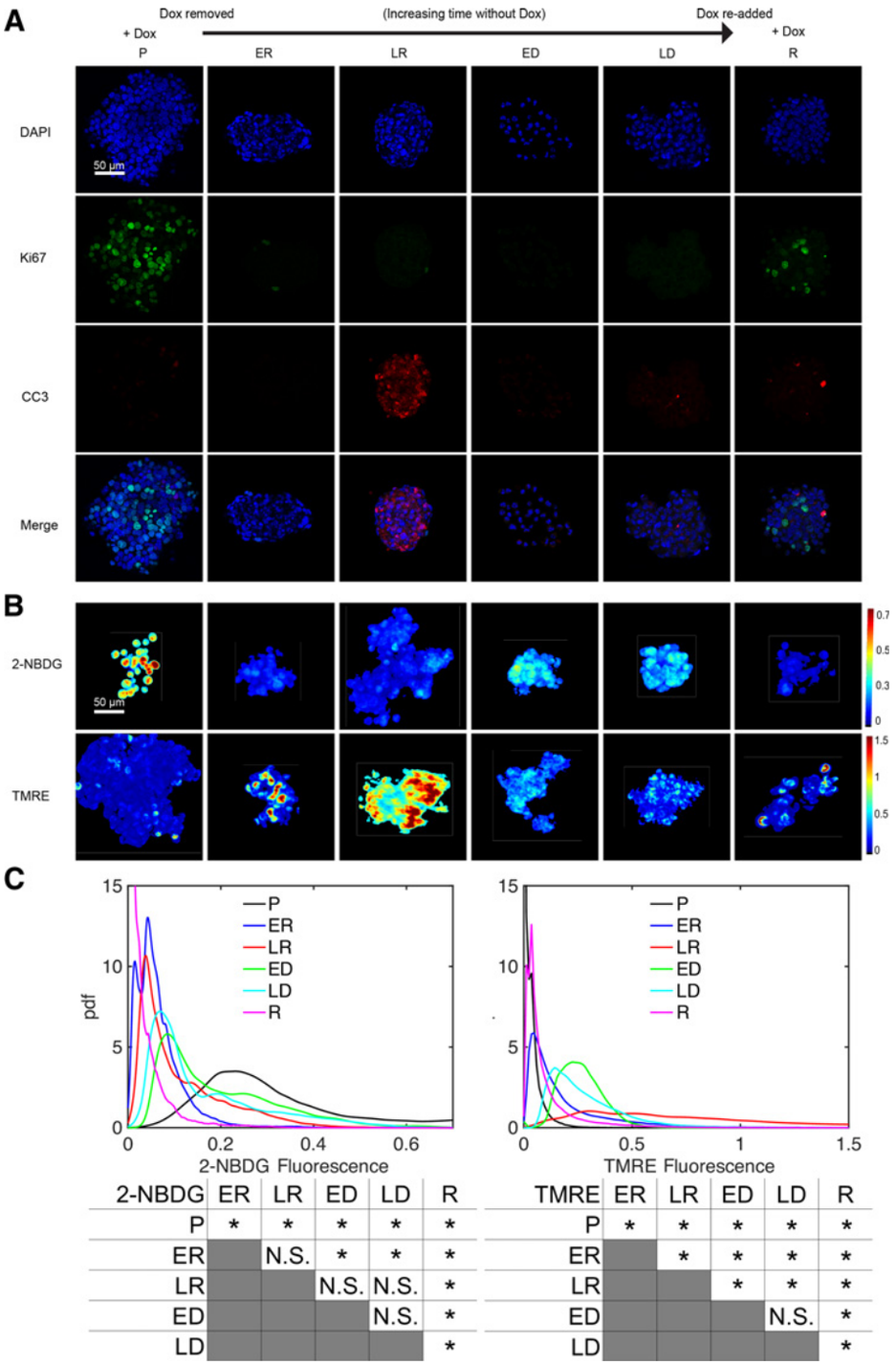

Figure 4.

Tumor metabolism reprograms during the different stages of a tumor's life cycle. Mammospheres stained for either Ki67 and CC3, 2-NBDG, or TMRE were imaged from cultures with doxycycline in the media (primary, P), without doxycycline in the media for 2 days prior to imaging (early regression, ER), without doxycycline in the media for 4 days prior to imaging (late regression, LR), without doxycycline in the media for 14 days prior to imaging (early residual disease, ED), and without doxycycline in the media for 28 days prior to imaging (late residual disease, LD). Cells were also cultured without doxycycline for 21 days followed by doxycycline added back in for 7 days (regrowth, R). **A,** Representative image planes of DAPI, Ki67, CC3 staining. **B,** Representative mean projection images of 2-NBDG and TMRE intensities. **C,** pdfs of 2-NBDG and TMRE intensities from the 3D mammospheres show significantly decreased 2-NBDG and significantly increased TMRE uptake after doxycycline withdrawal. After readdition of doxycycline to dormant tumors, 2-NBDG uptake remains significantly decreased. Significant comparisons between time points for both 2-NBDG and TMRE are included. For all groups, $n = 10$ mammospheres. (*, $P < 0.05$; N.S., not significant).

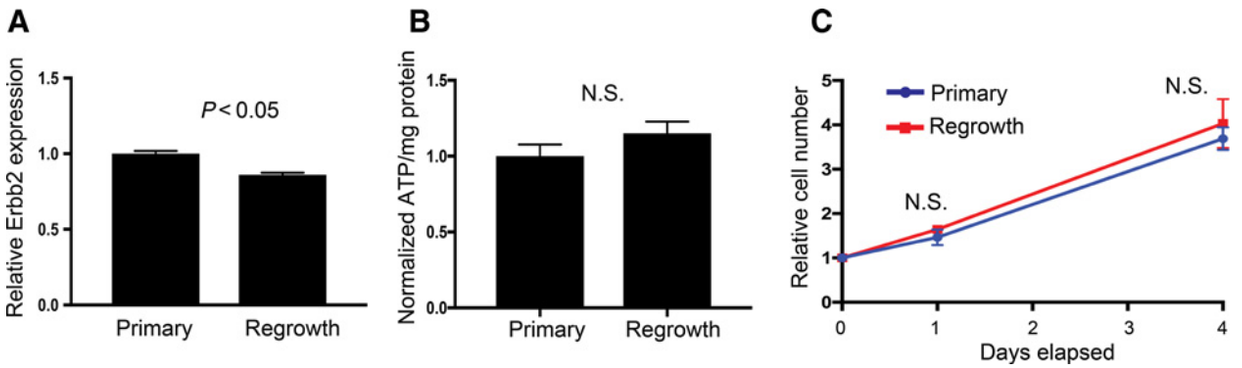

Figure 5.

ATP production, Her2 expression, and proliferation rate comparing mammospheres continuously cultured with doxycycline and no doxycycline 21 days + doxycycline 7 days (primary vs. regrowth). Mammospheres were either continuously cultured with doxycycline (primary) or removed from doxycycline for 21 days followed by the readdition of doxycycline for 7 days prior to assays (regrowth). **A,** qRT-PCR was used to measure Erbb2 (Her2) expression. Both primary and regrowth cultures show elevated Errb2 expression. For both groups, $n = 3$ biological replicates with three technical replicates. **B,** CellTiter-Glo was used to measure ATP production normalized to protein content and show no significant difference between primary and regrowth time points. For both groups, $n = 3$ biological replicates. **C,** Growth rate curves show no difference in proliferation between the two time points. For all groups, $n = 3$ biological replicates. Bars and markers are shown as the mean ± SEM (*, $P < 0.05$; N.S., not significant).

technique with the ability to link *in vitro* and *in vivo* results in biomedical research. Currently, gold standard techniques fail to directly connect *in vitro* cell culture results to preclinical *in vivo* models without changing endpoints. For example, the Seahorse Bioscience extracellular flux analyzer, the gold standard for metabolic studies *in vitro*, uses special perturbations to measure oxygen consumption rate to indicate oxidative phosphorylation and extracellular acidification rate to indicate glycolysis (50); however, this technique lacks the spatial information provided by imaging techniques such as the methodology described here. To move *in vivo*, typically FDG-PET or hyperpolarized MRI is used. FDG-PET is widely used to image glucose uptake, leaving out methods of measuring mitochondrial metabolism completely, and hyperpolarized MRI is used to image hyperpolarized carbon compounds to report on glycolysis or mitochondrial metabolism endpoints. This piecemeal approach does not allow for direct comparison between models across both glycolytic and mitochondrial pathways. Metabolic imaging using 2-NBDG and TMRE is advantageous to fill this void due to its ability to directly measure key pathways in metabolism and translate endpoints *in vitro*, as in this study, to *in vivo* models. In addition, the use of 3D confocal microscopy with a thin (3 μm) sectioning depth followed by a 3D segmentation algorithm in this study allowed for the uptake of either probe throughout the full mammosphere to be captured and compared across time points.

A GEM mouse model was chosen due to its relevance to the current metabolic research community and its consistent, well-defined timeline for studying different stages of tumor progression, treatment, dormancy, and recurrence (15, 34, 36, 37). To asses our method's ability to metabolically differentiate these life stages, we performed immunofluorescent staining of Ki67 and CC3 in parallel. These metrics highlighted the changes in phenotype across the time course with and without doxycycline: highly proliferative periods due to Her2 overexpression in primary and regrowing mammospheres, high levels of apoptosis following acute Her2 withdrawal mimicking a treatment response, and viable mammospheres lacking proliferative or apoptotic behavior following long-term Her2 downregulation modeling stable residual disease. Importantly, glucose uptake and mitochondrial membrane potential collectively allowed for differentiation between these time points highlighted by the differing immunofluorescent staining phenotypes. During initial doxycycline withdrawal, 2-NBDG uptake decreased ($P < 0.05$), which is consistent with a previous study in this model that reports a decrease in FDG-PET following acute doxycycline withdrawal (15). Also, TMRE uptake is significantly increased during early regression ($P < 0.05$) and again further during late regression ($P < 0.05$). In addition, during late regression, CC3 expression is increased ($P < 0.05$). In support of these observations, following acute doxycycline withdrawal in a similar model, populations of cells reported increased CC3 expression and an upregulation of the oxidative phosphorylation pathway (17). Another possibility, however, could be that this initial hyperpolarization seen in the early regression time point could be the beginning of the apoptotic pathway. Several studies have shown that hyperpolarization of the mitochondrial inner membrane can precede a depolarization step that catalyzes caspase 3 activity (51–53).

In the late regression phase (4 days off doxycycline), mammospheres showed their highest levels of both TMRE uptake ($P < 0.05$) and CC3 expression. At this point, many cells are likely under stress from acute Her2 downregulation resulting in high CC3 expression (49, 54, 55). Further analysis of the late regression population highlights the existence of two populations of cells: a high TMRE nonapoptotic cell population and a low TMRE population of apoptotic cells (Supplementary Fig. S5). Furthermore, it has previously been established that apoptosis and caspase 3 activity are both associated with a loss of mitochondrial membrane potential, or depolarization prior to cell death (56–58). Because of this, the increase in mitochondrial membrane potential measured by TMRE uptake in these mammospheres may be linked to a population of cells transitioning to a larger reliance on mitochondrial metabolism over glycolysis to survive Her2 downregulation. In fact, previous work has indicated that hyperpolarization of the mitochondrial membrane is a potential method to avoid apoptosis and that cancer cells with a high mitochondrial membrane potential report a heightened

tolerance to treatment (32, 59). Particular cells within the mammospheres could be rewiring their metabolism following doxycycline withdrawal as a tactic to survive the harsh conditions of oncogene downregulation. This switch is consistent with a pancreatic cancer study implicating a reliance on mitochondrial metabolism to survive periods of regression (60). 2-NBDG and TMRE together not only differentiated baseline from regression but also illustrated a dynamic metabolic process of cells undergoing metabolic adaptations and potentially showing a deterrent mechanism to escape cell death. The population of cells that remained viable 14 days following doxycycline withdrawal resisted apoptosis and were deemed residual diseased cells.

These surviving mammospheres cultured without doxycycline for 14 and 28 days showed no Ki67 or CC3 expression, further indicating their label as residual disease. Having already survived Her2 downregulation, these cells did not show as extreme TMRE uptake levels as the late regression mammospheres reported ($P < 0.05$), but their levels were higher than primary tumors, indicating a switch to oxidative phosphorylation instead of only glycolysis ($P < 0.05$). They also maintained a moderate level of 2-NBDG uptake, indicating the use of glucose as a fuel source for the citric acid cycle. This trend held for both time points and highlights the changes in preferred metabolic pathways required for long-term survival in Her2-downregulated environments. This is consistent with previous work, which indicated a switch to oxidative phosphorylation from glycolysis during dormancy (60).

We hypothesized that upon readdition of doxycycline to dormant mammospheres to induce regrowth, the metabolic phenotype of these mammospheres would be indistinguishable from baseline, primary mammospheres. Therefore, the finding that regrowing mammospheres exhibit reduced 2-NBDG uptake compared with all time points while also reporting a lower TMRE uptake compared with all time points off doxycycline was surprising. To rule out trivial differences between primary and regrowing mammospheres, ATP content, HER2 expression, and growth rate were measured. Primary and regrowing mammospheres reported similar ATP output and HER2 expression. Further, both time points showed no difference in Ki67 expression levels and the same growth rate, indicating a return to a highly proliferative phenotype. The cells that survived long-term Her2 downregulation were still responsive to doxycycline and behaved similarly to baseline mammospheres consistently cultured with doxycycline, except with respect to their glucose uptake and mitochondrial membrane potential.

Therefore, it is likely that these regrowing mammospheres have a distinct metabolic profile from primary mammospheres. Regrowing mammospheres exhibited the lowest glucose uptake compared with all other time points ($P < 0.05$). In addition, these mammospheres showed a decrease in mitochondrial membrane potential compared with residual disease ($P < 0.05$) and increase compared with primary mammospheres ($P < 0.05$). Although the mechanistic basis for this remains unknown, it suggests that the process of regression, dormancy, and regrowth may have profound effects on tumor metabolism. These effects could be due to adaptive changes, or result from the selection for cells with altered metabolic pathways. (20). Previous studies have reported that oncogenic transformations can cause permanent changes to expression or activity levels of enzymes or transporters, which could have occurred with the readdition of doxycycline (14). One possibility for the decrease in glucose uptake is that after the readdition of doxycycline, cells switch the substrate used for energy. These substrates would provide carbon for oxidative phosphorylation, similar to how glucose did in the residual disease population. The tricarboxylic acid cycle can rely on a host of other sources of carbon besides glucose alone (14). A previous study showed an increase in fatty acid degradation or glutamine uptake following therapy (17, 61). Further study is required to determine the specific change in substrate between the baseline and recurrent mammospheres. It is important to note that our strategy can only report on the downstream effect of such substrates, increased or decreased mitochondrial membrane potential. To robustly report on this change in substrate, metabolomics, hyperpolarized magnetic resonance imaging, or more fluorescent substrate analogues, like Bodipy FL C16 to measure long-chain fatty acid uptake, should be employed to pinpoint this metabolic shift (20).

This, however, leaves the question of the decreased mitochondrial membrane potential levels in the regrowing cells compared with other time points reliant on oxidative phosphorylation instead of glycolysis alone. It is possible that the mammospheres retained metabolic memory of the pathways required to survive long-term Her2 downregulation and rewired their metabolism to more efficiently use resources thus requiring less mitochondrial membrane potential compared with other time points also energetically reliant on oxidative phosphorylation (residual disease population). This along with the use of an alternative substrate could serve as rationale for the equal ATP output between primary and regrowth mammospheres.

Upon further examination of the TMRE fluorescence distribution, there exist two peaks, signifying two populations of cells within the time point with differing mitochondrial membrane potential. Previous work has shown increased heterogeneity in recurrent or relapsed tumors due to treatment-induced mutations or clonal evolution (62, 63). One possibility is that the cells with depressed mitochondrial membrane potential could be in the initial stages of apoptosis. As these mammospheres begin to recur, there is likely another selection process for the strongest cells to adapt to proliferate and survive, similar to the transition seen from regression to residual disease. It is likely that some residual cells cannot make the metabolic changes required for survival after the reexpression of Her2 (56). Following the death of these cells, the overall mitochondrial membrane potential of the population would increase. This unstable population may be a key metabolic window to target for future treatment studies due to their susceptibility to death (59). Further work should also be completed to examine the differences in the primary mammospheres compared with these two metabolic phenotypes within the regrowth cultures to identify key pathways involved with acquired drug resistance to Her2 therapies. Not only could these high membrane potential cells found in the regrowth population serve as potential therapy targets for metabolic inhibitors as key substrates are identified, but also this work indicates that mitochondrial membrane potential could serve as a metric to identify recurrent populations for further study.

A final possibility that could explain the metabolic differences between primary mammospheres and regrowing cells is that the latter cells were exposed to Her2 signaling for a shorter period of time. That is, the metabolism of these regrowing cells could still be changing, and they may eventually resemble more

closely the primary tumor cells. This, in turn, would suggest the intriguing possibility that the metabolic profile of tumors at early stages of recurrence is unique and may provide opportunities for therapeutic intervention.

Metabolism is highly dependent on the surrounding environment. Although *in vitro* culture is critically important in modern cancer research, it cannot fully replicate the tumor microenvironment and the role of vasculature in these tumor stages. Finally, caution should be considered regarding the use of TMRE, because it is directly correlated to mitochondrial membrane potential but does not explicitly report on a voltage due to the proton gradient; our method relies on a relative measurement. Next steps to further understand the transition of metabolism occurring within a tumor's life should be to image each stage with 2-NBDG and TMRE *in vivo* using a GEM-derived mammary transplant and a mammary window chamber. These methods still allow for the high resolution seen with the mammospheres but include other valuable sources of information such as hemoglobin saturation and angiogenesis to aid in a deeper understanding of aerobic respiration's role in dormant and recurrent populations and the tumor's interplay with tumor-associated fibroblasts. In addition, we have shown here that 2-NBDG and TMRE can be used to stain superficial cell aggregates, but the limitations of dye permeability in larger cell aggregates *in vitro* remains uncharacterized. Finally, the use of 3D confocal microscopy was selected for this study to reduce out-of-focus fluorescence and multi-scattering events in each image; however, scattering may still affect fluorescence as a function of depth. The work described here presents a new technique for the direct study of two key metabolic endpoints related to tumor metabolism and has the potential to be expanded to image other endpoints in the future.

Disclosure of Potential Conflicts of Interest

No potential conflicts of interest were disclosed.

Disclaimer

The funders had no role in study design, data collection and analysis, decision to publish, or preparation of the manuscript.

Authors' Contributions

Conception and design: M.C. Madonna, D.B. Fox, B.T. Crouch, J.V. Alvarez, N. Ramanujam

Development of methodology: M.C. Madonna, D.B. Fox, B.T. Crouch, A.F.Martinez, J.V. Alvarez, N. Ramanujam

Acquisition of data (provided animals, acquired and managed patients, provided facilities, etc.): M.C. Madonna, D.B. Fox

Analysis and interpretation of data (e.g., statistical analysis, biostatistics, computational analysis): M.C. Madonna, D.B. Fox, B.T. Crouch, J. Lee, C. Zhu, A.F.Martinez, J.V. Alvarez, N. Ramanujam

Writing, review, and/or revision of the manuscript: M.C. Madonna, D.B. Fox, B.T. Crouch, C. Zhu, A.F.Martinez, J.V. Alvarez, N. Ramanujam

Administrative, technical, or material support (i.e., reporting or organizing data, constructing databases): M.C. Madonna, J. Lee

Study supervision: J.V. Alvarez, N. Ramanujam

Acknowledgments

This work is supported by generous funding from Duke School of Medicine Core Facility Voucher Program, NIH grant 1R01CA195500-01, V Foundation grant, and the Duke Medical Imaging Training Program NIH grant T32-EB001040. Thanks to Dr. Yasheng Gao at Duke University's Light Microscopy Core Facility for imaging troubleshooting. Many thanks to Dr. Brandon Nichols for the discussion of image-processing methodologies and Marianne Lee for assistance in preliminary experiments.

Received June 11, 2018; revised October 9, 2018; accepted March 19, 2019; published first March 22, 2019.

References

1. Howlader N, Noone AM, Krapcho M, Miller D, Bishop K, Kosary CL, et al. SEER cancer statistics review, 1975-2014. Bethesda, MD: NCI; 2017.
2. Gonzalez-Angulo AM, Litton JK, Broglio KR, Meric-Bernstam F, Rakkhit R, Cardoso F, et al. High risk of recurrence for patients with breast cancer who have human epidermal growth factor receptor 2-positive, node-negative tumors 1 cm or smaller. J Clin Oncol 2009;27:5700–6.
3. Buzdar AU, Ibrahim NK, Francis D, Booser DJ, Thomas ES, Theriault RL, et al. Significantly higher pathologic complete remission rate after neoadjuvant therapy with trastuzumab, paclitaxel, and epirubicin chemotherapy: results of a randomized trial in human epidermal growth factor receptor 2-positive operable breast cancer. J Clin Oncol 2005;23:3676–85.
4. Debska-Szmich S, Krakowska M, Czernek U, Habib-Lisik M, Zieba A, Potemski P. The role of preoperative systemic treatment in patients with breast cancer. Contemp Oncol 2016;20:93–101.
5. Symmans WF, Peintinger F, Hatzis C, Rajan R, Kuerer H, Valero V, et al. Measurement of residual breast cancer burden to predict survival after neoadjuvant chemotherapy. J Clin Oncol 2007;25:4414–22.
6. Mougalian SS, Hernandez M, Lei X, Lynch S, Kuerer HM, Symmans WF, et al. Ten-year outcomes of patients with breast cancer with cytologically confirmed axillary lymph node metastases and pathologic complete response after primary systemic chemotherapy. JAMA Oncol 2016;2:508–16.
7. Wuerstlein R, Harbeck N. Neoadjuvant therapy for HER2-positive breast cancer. Rev Recent Clin Trials 2017;12:81–92.
8. Hayashi N, Takahashi Y, Matsuda N, Tsunoda H, Yoshida A, Suzuki K, et al. The prognostic effect of changes in tumor stage and nodal status after neoadjuvant chemotherapy in each primary breast cancer subtype. Clin Breast Cancer 2018;18:e219–29.
9. Diel I, Kaufmann M, Costa SD, Holle R, von Minckwitz G, Solomayer EF, et al. Micrometastatic breast cancer cells in bone marrow at primary surgery: prognostic value in comparison with nodal status. J Natl Cancer Inst. 1996;88:1652–8.
10. Saphner T, Tormey D, Gray R. Annual hazard rates of recurrence for breast cancer after primary therapy. J Clin Oncol 1996;14:2738–46.
11. Symmans WF, Wei C, Gould R, Yu X, Zhang Y, Liu M, et al. Long-term prognostic risk after neoadjuvant chemotherapy associated with residual cancer burden and breast cancer subtype. J Clin Oncol 2017;35:1049–60.
12. Weinberg SE, Chandel NS. Targeting mitochondria metabolism for cancer therapy. Nat Chem Biol 2015;11:9–15.
13. Nagarajan A, Malvi P, Wajapeyee N. Oncogene-directed alterations in cancer cell metabolism. Trends Cancer 2016;2:365–77.
14. Keenan MM, Chi JT. Alternative fuels for cancer cells. Cancer J 2015;21:49–55.
15. Alvarez JV, Belka GK, Pan TC, Chen CC, Blankemeyer E, Alavi A, et al. Oncogene pathway activation in mammary tumors dictates FDG-PET uptake. Cancer Res 2014;74:7583–98.
16. Bjurberg M, Gustavsson A, Ohlsson T, Brun E. FDG-PET in the detection of residual disease and relapse in patients with Hodgkin's lymphoma. Experience from a Swedish centre. Acta Oncol 2006;45:743–9.
17. Havas KM, Milchevskaya V, Radic K, Alladin A, Kafkia E, Garcia M, et al. Metabolic shifts in residual breast cancer drive tumor recurrence. J Clin Invest 2017;127:2091–105.
18. Scatena R, Bottoni P, Giardina B. Mitochondria, metabolism and cancer: a growing role in cancer cell differentiation and cancer cell dormancy. Cancer Metab 2014;2:P64.
19. Kurmi K, Hitosugi S, Yu J, Boakye-Agyeman F, Wiese EK, Larson TR, et al. Tyrosine phosphorylation of mitochondrial creatine kinase 1 enhances a druggable tumor energy shuttle pathway. Cell Metab 2018;28:833–47.
20. Youn H, Hong KJ. In vivo non invasive molecular imaging for immune cell tracking in small animals. Immune Netw 2012;12:223–9.

21. Solomon M, Liu Y, Berezin MY, Achilefu S. Optical imaging in cancer research: basic principles, tumor detection, and therapeutic monitoring. Med Princ Pract 2011;20:397–415.
22. Hou J, Wright HJ, Chan N, Tran R, Razorenova OV, Potma EO, et al. Correlating two-photon excited fluorescence imaging of breast cancer cellular redox state with seahorse flux analysis of normalized cellular oxygen consumption. J Biomed Opt 2016;21:60503.
23. Zhu C, Martinez AF, Martin HL, Li M, Crouch BT, Carlson DA, et al. Near-simultaneous intravital microscopy of glucose uptake and mitochondrial membrane potential, key endpoints that reflect major metabolic axes in cancer. Sci Rep 2017;7:13772.
24. Rajaram N, Frees AE, Fontanella AN, Zhong J, Hansen K, Dewhirst MW, et al. Delivery rate affects uptake of a fluorescent glucose analog in murine metastatic breast cancer PLoS One 2013;8:e76524.
25. Millon SR, Ostrander JH, Brown JQ, Raheja A, Seewaldt VL, Ramanujam N. Uptake of 2-NBDG as a method to monitor therapy response in breast cancer cell lines. Breast Cancer Res Treat 2011;126:55–62.
26. Frees AE, Rajaram N, McCachren SS, Fontanella AN, Dewhirst MW, Ramanujam N. Delivery-corrected imaging of fluorescently-labeled glucose reveals distinct metabolic phenotypes in murine breast cancer. PloS One 2014;9:e115529.
27. Rajaram N, Reesor AF, Mulvey CS, Frees AE, Ramanujam N. Non-invasive, simultaneous quantification of vascular oxygenation and glucose uptake in tissue. Plos One 2015;10:e0117132.
28. Yamada K, Saito M, Matsuoka H, Inagaki N. A real-time method of imaging glucose uptake in single, living mammalian cells. Nat Protoc 2007;2: 753–62.
29. Tsytsarev V, Maslov KI, Yao J, Parameswar AR, Demchenko AV, Wang LV. In vivo imaging of epileptic activity using 2-NBDG, a fluorescent deoxyglucose analog. J Neurosci Methods 2012;203:136–40.
30. Cai HW, Peng FY.2-NBDG fluorescence imaging of hypermetabolic circulating tumor cells in mouse xenograft model of breast cancer. J Fluoresc 2013;23:213–20.
31. Perry SW, Norman JP, Barbieri J, Brown EB, Gelbard HA. Mitochondrial membrane potential probes and the proton gradient: a practical usage guide. Biotechniques 2011;50:98–115.
32. Martinez AF, McCachren SS 3rd, Lee M, Murphy HA, Zhu C, Crouch BT, et al. Metaboloptics: visualization of the tumor functional landscape via metabolic and vascular imaging. Sci Rep 2018;8:4171.
33. Moody SE, Sarkisian CJ, Hahn KT, Gunther EJ, Pickup S, Dugan KD, et al. Conditional activation of Neu in the mammary epithelium of transgenic mice results in reversible pulmonary metastasis. Cancer Cell 2002;2: 451–61.
34. Feng Y, Pan TC, Pant DK, Chakrabarti KR, Alvarez JV, Ruth JR, et al. SPSB1 promotes breast cancer recurrence by potentiating c-MET signaling. Cancer Discov 2014;4:790–803.
35. Alvarez JV, Pan TC, Ruth J, Feng Y, Zhou A, Pant D, et al. Par-4 down-regulation promotes breast cancer recurrence by preventing multinucleation following targeted therapy. Cancer Cell 2013;24:30–44.
36. Moody SE, Perez D, Pan TC, Sarkisian CJ, Portocarrero CP, Sterner CJ, et al. The transcriptional repressor Snail promotes mammary tumor recurrence. Cancer Cell 2005;8:197–209.
37. Abravanel DL, Belka GK, Pan TC, Pant DK, Collins MA, Sterner CJ, et al. Notch promotes recurrence of dormant tumor cells following HER2/neu-targeted therapy. J Clin Invest 2015;125:2484–96.
38. Slamon D, Clark G, Wong S, Levin W, Ullrich A, McGuire W. Human breast cancer: correlation of relapse and survival with amplification of the HER-2/neu oncogene. Science 1987;235:177–82.
39. Scaduto R, Grotyohann L. Measurement of mitochondrial membrane potential using fluorescent rhodamine derivatives. Biophys J 1999;76: 469–77.
40. Martinez A, McCachren SS 3rd, Lee M, Murphy HA, Zhu C, Crouch BT, et al. Metaboloptics: visualization of the tumor functional landscape via metabolic and vascular imaging. Sci Rep 2018;8:4171.
41. O'Neil RG, Wu L, Mullani N. Uptake of a fluorescent deoxyglucose analog (2-NBDG) in tumor cells. Mol Imaging Biol 2005;7:388–92.
42. Crowley LC, Christensen ME, Waterhouse NJ. Measuring mitochondrial transmembrane potential by TMRE staining. Cold Spring Harb Protoc 2016;2016;087361.
43. Sethian JA. Level set methods and fast marching methods: evolving interfaces in computational geometry, fluid mechanics, computer vision, materials science. Cambridge, UK: Cambridge University Press; 1999.
44. Aguirre GK, Zarahn E, D'Esposito M. A critique of the use of the Kolmogorov-Smirnov (KS) statistic for the analysis of BOLD fMRI data. Magnetic Resonance Med 1998;39:500–5.
45. Lombardo Y, de Giorgio A, Coombes CR, Stebbing J, Castellano L. Mammosphere formation assay from human breast cancer tissues and cell lines. J Vis Exp 2015;97:52671.
46. Wang R, Lv Q, Meng W, Tan Q, Zhang S, Mo X, et al. Comparison of mammosphere formation from breast cancer cell lines and primary breast tumors. J Thorac Dis 2014;6:829–37.
47. Vander Heiden MG, Plas DR, Rathmell JC, Fox CJ, Harris MH, Thompson CB. Growth factors can influence cell growth and survival through effects on glucose metabolism. Mol Cell Biol 2001;21: 5899–912.
48. Bos R, van Diest PJ, de Jong JS, van der Groep P, van der Valk P, van der Wall E. Hypoxia-inducible factor-1alpha is associated with angiogenesis, and expression of bFGF, PDGF-BB, and EGFR in invasive breast cancer. Histopathology 2005;46:31–6.
49. Kannan K, Jain S. Oxidative stress and apoptosis. Pathophysiology 2000;7:153–63.
50. TeSlaa T, Teitell MA. Techniques to monitor glycolysis. Methods Enzymol 2014;542:91–114.
51. Banki K, Hutter E, Gonchoroff NJ, Perl A. Elevation of mitochondrial transmembrane potential and reactive oxygen intermediate levels are early events and occur independently from activation of caspases in Fas signaling. J Immunol 1999;162:1466–79.
52. Jo WS, Jeong MH, Jin YH, Jang JY, Nam BH, Son SH, et al. Loss of mitochondrial membrane potential and caspase activation enhance apoptosis in irradiated K562 cells treated with herbimycin A. Int J Radiat Biol 2005;81:531–43.
53. Perl A, Gergely P Jr, Nagy G, Koncz A, Banki K. Mitochondrial hyperpolarization: a checkpoint of T-cell life, death and autoimmunity. Trends Immunol 2004;25:360–7.
54. Takahashi A, Masuda A, Sun M, Centonze VE, Herman B. Oxidative stress-induced apoptosis is associated with alterations in mitochondrial caspase activity and Bcl-2-dependent alterations in mitochondrial pH (pHm). Brain Res Bull 2004;62:497–504.
55. Satoh T, Enokido Y, Aoshima H, Uchiyama Y, Hatanaka H. Changes in mitochondrial membrane potential during oxidative stress-induced apoptosis in PC12 cells. J Neurosci Res 1997;50:413–20.
56. Heiskanen KM, Bhat MB, Wang HW, Ma J, Nieminen AL. Mitochondrial depolarization accompanies cytochrome c release during apoptosis in PC6 cells. J Biol Chem 1999;274:5654–8.
57. Zamzami N, Marchetti P, Castedo M, Decaudin D, Macho A, Hirsch T, et al. Sequential reduction of mitochondrial transmembrane potential and generation of reactive oxygen species in early programmed cell death. J Exp Med 1995;182:367–77.
58. Gutscher M, Pauleau AL, Marty L, Brach T, Wabnitz GH, Samstag Y, et al. Real-time imaging of the intracellular glutathione redox potential. Nat Methods 2008;5:553–9.
59. Zhang BB, Wang DG, Guo FF, Xuan C. Mitochondrial membrane potential and reactive oxygen species in cancer stem cells. Fam Cancer 2015;14: 19–23.
60. Viale A, Pettazzoni P, Lyssiotis CA, Ying H, Sánchez N, Marchesini M, et al. Oncogene ablation-resistant pancreatic cancer cells depend on mitochondrial function. Nature 2014;514:628–32.
61. Fan J, Kamphorst JJ, Mathew R, Chung MK, White E, Shlomi T, et al. Glutamine-driven oxidative phosphorylation is a major ATP source in transformed mammalian cells in both normoxia and hypoxia. Mol Syst Biol 2013;9:712.
62. Johnson BE, Mazor T, Hong C, Barnes M, Aihara K, McLean CY, et al. Mutational analysis reveals the origin and therapy-driven evolution of recurrent glioma. Science 2014;343:189–93.
63. Ding L, Ley TJ, Larson DE, Miller CA, Koboldt DC, Welch JS, et al. Clonal evolution in relapsed acute myeloid leukaemia revealed by whole-genome sequencing. Nature 2012;481:506–10.